Article:
Al-Damook, A, Kapur, N, Summers, JL et al. (2015) An experimental and computational investigation of thermal air flows through perforated pin heat sinks. Applied Thermal Engineering, 89. 365 - 376. ISSN: 1359-4311

https://doi.org/10.1016/j.applthermaleng.2015.06.036

An experimental and computational investigation of thermal air flows through perforated pin heat sinks

Amer. Al-Damook[1,2,*], N. Kapur[1], J.L. Summers[1], H.M. Thompson[1]
[1]School of Mechanical Engineering, University of Leeds, UK
[2]Mechanical Engineering Department, Faculty of Engineering, University of Anbar, Iraq,
*Corresponding Author/ mnajs@leeds.ac.uk/ +447741695880

ABSTRACT

The benefits of using pin fin heat sinks with multiple perforations are investigated using complementary experimental and Computational Fluid Dynamics (CFD) methods. An experimental heat sink with multiple perforations is designed and fabricated and parameter studies of the effect of perforated pin fin design on heat transfer and pressure drops across the heat sinks undertaken. Experimental data is found to agree well with predictions from a CFD model for the conjugate heat transfer into the cooling air stream. The validated CFD model is used to carry out a parametric study of the influence of the number and positioning of circular perforations, which shows that the Nusselt number increases monotonically with the number of pin perforations, while the pressure drop and fan power required to overcome the pressure drop all reduce monotonically. Pins with five perforations are shown to have a 11% larger Nu than for corresponding solid pin cases. These benefits arise due to not only the increased surface area but also heat transfer enhancement near perforations through the formation of localised air jets. In contrast, the locations of the pin perforations are much less influential. When examined in the context of CPU cooling, a conjugate heat transfer analysis shows that improved heat transfer with pin perforations translates into significantly reduced processor case temperatures with the additional benefit of a reduction in the weight of the heat sink's pins. To achieve these benefits care must be taken to ensure that pin perforations are aligned with the dominant flow direction and manufactured with a good quality surface finish.

HIGHLIGHTS

- The cooling critical components by pin fin heat sinks.
- The substantial performance benefits via use of multiple pin perforations.
- Enhancement heat transfer and fan power of pinned heat sinks.
- Conjugate heat transfer and turbulent airflow model.

NOMENCLATURE			
A_c	cross-sectional area of the flow passage of the heat sink, m^2	Re	Reynolds number
D	pin diameter of the pin fin heat sink, mm	T	temperature, ^oC
d	perforation diameter of the pin fin, mm	ΔT	temperature difference, ^oC
D_h	hydraulic diameter, m	U	air velocity, m/s
H	pin fin height, mm	**Greek**	
h	heat transfer coefficient, $W/m^2.K$	α	fluid thermal diffusivity (m^2/s)
k	turbulence kinetic energy	α,β,β^*	turbulence model constant
n	number of perforations	ϕ	porosity $V_{void}=V$
N	number of pins	μ	fluid viscosity (Pa·s)
L	heat sink length, mm	μ_t	turbulent eddy viscosity, Pa.s
Nu	Nusselt number	ρ	fluid density (kg/m^3)
P	fan power, W	νt	kinematic viscosity, m^2/s
Δp	pressure drop, Pa	$_{vt}$	turbulent kinematic viscosity, m^2/s
Pr	Prandtl number	σ_ε	k-ε turbulence model constant
Pr_t	turbulent Prandtl number	σ	turbulence model constant for the k-equation
Q	power applied on the base, W	ω	k-ω turbulence model constant
S_z	pin pitch in streamwise direction, mm		

1. INTRODUCTION

Many industrial systems have critical components which must be cooled at a rate sufficient to avoid serious overheating problems and system failures. Convective heat transfer to heat sinks with extended surface fins provides the required heat transfer management in several important applications, including engines and turbine blades in the aerospace industry, automotive vehicle heat exchangers and gas-cooled nuclear reactors, Sahin et al [1, 2]. At a smaller scale, convective heat transfer to air as it flows over a network of fins is also the most common approach to cooling microelectronics due to is low cost, availability and reliability, Zhou & Catton [3]. The surface fins offer a practical means of achieving large heat transfer area, without excessive primary surface area, and act as turbulence promoters thus further enhancing heat transfer rates. The main design goals for such heat sinks are usually to maximise heat transfer rates for minimal pressure loss. Further details are available in the recent review by Nagarani et al [4].

Plate fin heat sinks (PFHSs) are widely used due to their simple structure and ease of manufacturing. Although many optimisation studies have been carried out for plate fin heat sinks, see e.g. Chiang's [5] experimental optimisation using Taguchi methods, they cannot overcome the intrinsic limitation that air flows smoothly through the heat sink channels, due to the parallel plate arrangement, limiting the achievable heat transfer rates. Pin fin heat sinks (PFHSs) can be an effective alternative to plate fin heat sinks since they have the advantage of hindering the development of the thermal boundary layer on smooth surfaces responsible for limiting the heat transfer rates in plate fin designs, Zhou & Catton [3]. Several previous investigations of heat transfer and pressure drops of PFHSs have demonstrated clearly their superiority over plate fin designs and have attempted to optimise these by studying, for

example, the effect of pin cross-sectional shape Soodphakdee et al [6], Jonsson & Moshfeghor [7] and the benefits of combining plate and pin fins within compound heat sinks, Yang & Peng [8, 9].

The increasing focus on energy-efficiency and environmental sustainability, together with the need to achieve higher cooling densities, are providing strong drivers to optimize the performance of cooling technologies for a range of applications. Recent studies have demonstrated the potential of using highly conductive inserts to provide efficient pathways for heat removal from electronic components, Hajmohammadi et al [10] and the role of optimal plate thicknesses in laminar forced convection cooling of heat sources, Hajmohammadi et al [11]. Of greater relevance to the present study are those that have focused on the optimization of plate fin heat sinks using computational and experimental methods. Examples of the former include the use of multi-objective Genetic Algorithms to optimize plate fin geometries for total heat transfer rate and total annual costs, Najafi et al [12], while the latter include the use of experimental Taguchi methods to optimize plate fin heat sinks with periodically interrupted diverging and converging fins Kotcioglu et al [13], which can enhance heat transfer significantly due to boundary layer disturbances and secondary mixing effect. The additional benefits of using multiple air streams in plate fin heat sinks have recently been reviewed by Kumar Das and Ghosh [14].

Recent experimental and computational studies have also shown that perforating plates and pins on heat sinks can offer significant benefits. Most studies have examined the benefits of perforating plate fins. Shaeri & Yaghoubi [15, 16] and Shaeri & Jen [17, 18], for example, studied the effect of the number of perforations and their size, while Farhad Ismail et al. [19, 20] considered the influence of perforation shape, on heat transfer and frictional drag on the air for both laminar and turbulent flow cases. Shaeri & Jen [17, 18], for example, found that a single perforation in a plate fin could increase the heat transfer rate by up to 80%. More generally, these studies found that increasing the number of perforations in plate fins leads to reductions in the size of the wakes behind the fin, the length of the recirculation zone around the lateral surface of the fin and in the total drag, where an increase in friction drag is compensated by a greater reduction in pressure drag. Dhanawade and Dhanawade [21] experimentally determined the effect of lateral circular perforations for plate fins on heat transfer. They found that perforations generally increase the Nusselt number and that the optimum perforation diameter is a function of the applied heat flux density, with larger perforations being beneficial for low heat fluxes and smaller perforations better for high heat fluxes.

In comparison with plate fins, relatively few studies have considered the effect of perforations on the heat transfer and pressure drop in PPHSs and those that have focused on the benefits of single perforations. Sahin and Demir [1, 2], for example, studied the effect of

the cross-section shape (circular or square) for in-line pin arrays, while Amol and Farkade [22] considered the effect of staggered pin arrangements for singly-perforated pins of circular cross-section. These have shown that localised jet flows through the perforations increase local heat transfer by alleviating the recirculation zones that form behind solid pins, increasing shear-induced mixing. These studies have found consistently that a single perforation leads to an enhancement in heat transfer and a reduction in pressure drop compared to equivalent solid pin systems. Another promising approach which can improve heat transfer rate and reduce pressure drop simultaneously, in both single-phase and two-phase systems, is to use a microjet to induce flow separation; see e.g. [23].

This study presents the first comprehensive experimental and computational investigation into the benefits of multiple pin fin perforations on the heat transfer and pressure drop in pin fin heat sinks. Experimental data is presented, for the first time, on the benefits of using multiple perforations and the data used to validate a corresponding Computational Fluid Dynamics (CFD) model of the conjugate heat transfer problem. The latter is then used to carry out a comprehensive parameter study into the effect of the number and distribution of pin fin perforations on the heat transfer and pressure drop in pin fin heat sinks. Section 2 describes the problems under consideration and experimental methods, section 3 the numerical methods and conjugate heat transfer model, while section 4 describes the validation of the CFD approach and the results of the parameter study. Conclusions are drawn in Section 5.

2. EXPERIMENTAL METHODS

2.1 Airflow Channel Section

An experimental rig system was designed and fabricated, consisting of a closed, rectangular channel in which the heat sink test section could be located, see Figure 1. The channel is constructed of clear Perspex of 8mm thickness and has an internal rectangular cross-section of width 50mm, height 10mm and total length 370mm. The heat sink is located at the centre of the straight channel section, a distance of 110mm from upstream entrance to the channel. A mini fan (model San Ace 36: 9GV3612P3J03) of size 36x36x28mm, 12VDC and 0.75A creates the airflow (19.4CFM) through the channel and over a heat sink. Metal meshes are positioned at a distance of 50mm either side of the heat sink to minimise flow mal-distribution and create a uniform airflow profile over the heat sink. The channel is equipped with tappings allowing the pressure drop across the heat sink to be measured by a digital manometer and insertion points allowing the change in temperature of the air to be recorded via a digital thermometer.

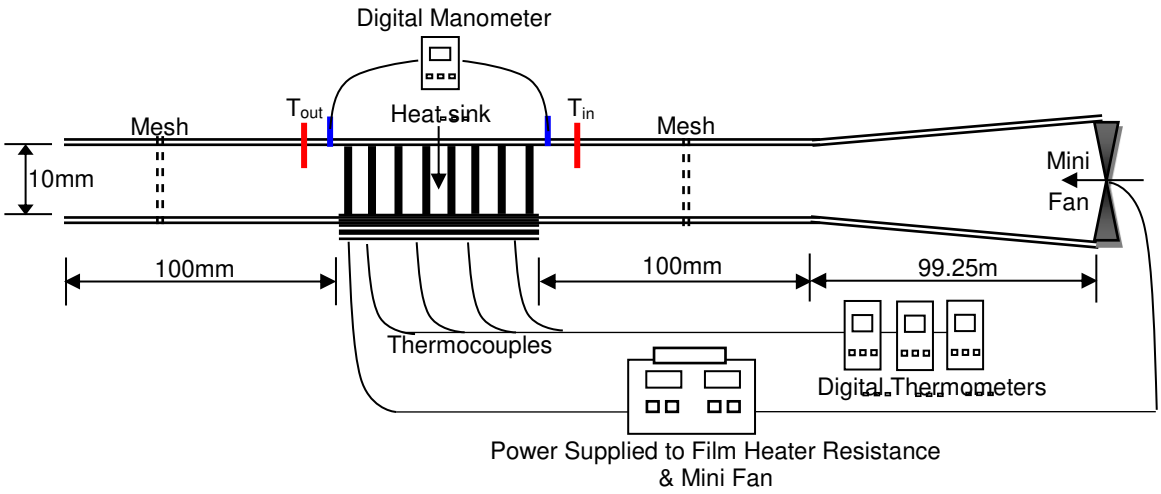

Figure 1: Schematic diagram of the experimental system.

2.2 Heat Sink and Test Section Design

Two heat sinks were fabricated from aluminium, the first with solid pins and the second with perforated pins – see figure 2. Each pin was cut from 2mm diameter aluminium bar using a rivet cutter to a length of 12mm. In the case of the perforated pins, a steel guide was used allowing 1mm holes to be drilled into the bar. The individual pins were brazed onto a 2mm square (50mm) base plate that was pre-drilled with a regular array of holes with 6.5mm spacing between centres in both directions. In the case of the perforated pins, the holes were aligned with the direction of the airflow.

The heat sink was installed into the flow channel using a removable test section (figure 3) consisting of a thick teflon plate, a layer of fibreglass insulation (that also wrapped around the edge of the test section) and a thin film heater bonded to the base of the heat sink using a thin layer (<1mm) of thermally conductive epoxy. The thin film heater was constructed from Nichrome resistance wire 2mm thickness coiled around mica sheet of 2.5mm spacing to reduce the load in the extend wires and provided good heat flux uniformity. The teflon plate acts as a backing plate to hold the composite heat sink and it is set into the flow test channel via four corner screws (figure 3). The heat input was determined from the voltage and current drawn by the thin film heater with a heat output of approximately 60W. K-type thermocouples were bonded into the base plate of the heat sink, allowing base temperatures to be measured. At the same time, other thermocouples are bonded at the upper surface of the heat sinks to determine the average upper surface temperature for calculating the heat transfer rate and Nusselt number. In all cases, the thermocouples were embedded by drilling a shallow indentation (~1mm) which holds the tip of the thermocouple, and thermally conductive epoxy resin applied to restore the surface geometry.

2.3 Experimental measurements and data analysis

Temperatures at the upper and lower surfaces of the heat sink are measured using thermocouples and the heat transfer rate and Nusselt number calculated using the known thermal conductivity of the heat sink. The inlet and outlet air temperatures are measured using

thermocouples at the entrance and exit of the heat sink and the pressure drop across the heat sink is measured using two pressure taps, located in front of and behind the heat sink, with pressure readings taken from a digital manometer. Finally, the inlet air velocity is measured using a hot wire anemometer.

The steady-state rate of heat transfer through the air can be expressed via

$$\dot{Q}_{elec} = \dot{Q}_{conv} + \dot{Q}_{rad} + \dot{Q}_{loss}.$$

$\dot{Q}_{elec} = IV$ is the total electrical power applied to the base of the heat sink and $\dot{Q}_{conv}$, $\dot{Q}_{rad}$ and $\dot{Q}_{loss}$ are the heat transfer rates from the heat sink by convection, radiation and through conductive losses, respectively. $\dot{Q}_{rad}$ is given by [24]

$$\dot{Q}_{rad} = \sigma F A_s \left(T_w^4 - T_a^4\right)$$

where F is the view factor. The pin fins and base plate of the heat sink are made of highly polished aluminium to reduce their emissivities and the experimental data showed that $\dot{Q}_{rad} / \dot{Q}_{elec} \approx 0.004$. $\dot{Q}_{rad}$ is therefore neglected in the results presented below.

Conductive heat losses are minimised by ensuring that all the outer walls of the heat sink are well-insulated. Thermocouple measurements of the heat sink outer wall temperatures confirm that the conductive losses are smaller than 2% of applied heat flux and that these are close to the ambient temperatures.

$\dot{Q}_{loss}$ is given by $\dot{Q}_{loss} = \frac{AK_{ins}}{\Delta X}.\Delta T_{ins}$ where A is the heat sink base area, K_{ins} is the thermal conductivity of the insulation, ΔT_{ins} the temperature difference across the insulation, and ΔX the insulation thickness.

The average convective heat transfer coefficient, h, and Nusselt number, Nu, are determined via the expressions [25, 34]:

$$h = \frac{\dot{Q}_{conv}}{A_s[T_w - (\frac{T_{out} + T_{in}}{2})]}, \quad Nu = \frac{hL}{k}$$

where T_w is the heat sink temperature at its upper surface, T_{in} and T_{out} are the average inlet and outlet air temperatures, respectively, and A_s is the surface area of the heat sink. Previous researchers have calculated h based on either the projected, A_P, or total, A_T, surface area of the heat sink and these are related to one another via the relationship $h_P = h_T(A_T/A_P)$.

For solid pin fins the total surface area $A_T = WL + N(\pi DH)$, where W and L are the width and length of the heat sink respectively and H, D and N are the height, diameter and number of pin fins respectively. For perforated pin fins $A_T = WL + \pi N(HD + ndD - nd/2)$, where n is the

number of perforations of diameter d on each pin fin. The Reynolds number and hydraulic diameter are defined respectively by $\mathrm{Re} = \frac{UD_h}{\nu}$, and $D_h = 4\frac{A_c}{p} = 2\frac{HW}{(H+W)}$.

The values of the thermo-physical properties of the air are obtained at the average bulk mean temperature $T_m=(T_{in}+T_{out})/2$. The pressure drop across the heat sink, $\Delta p=p_{in}-p_{out}$, is measured using a digital manometer and is an important quantity since the fan power required to overcome it is given by $P_{fan}=U.A.\Delta p$, where $A=H.S_z.(N-1)$ is the cross-sectional area of the flow passage of the heat sink and S_z is the uniform pin fin spacing.

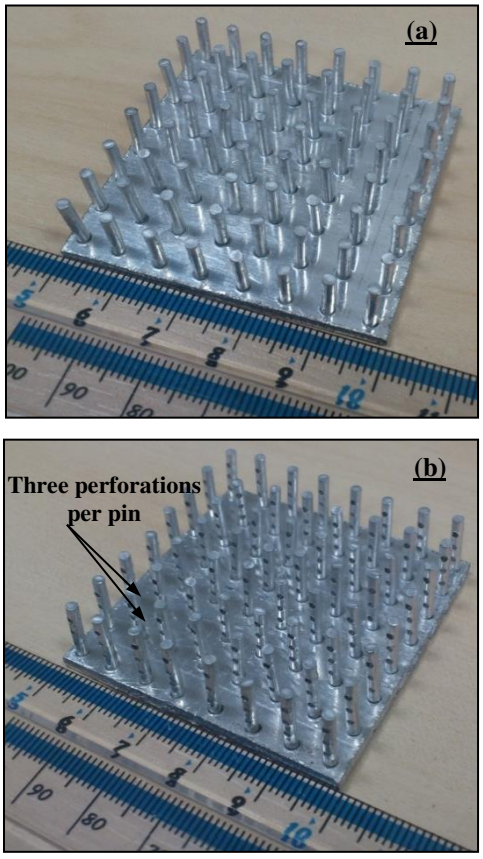

Figure 2: Final design of (A) solid pin fins and (B) perforated pin fins heat sinks

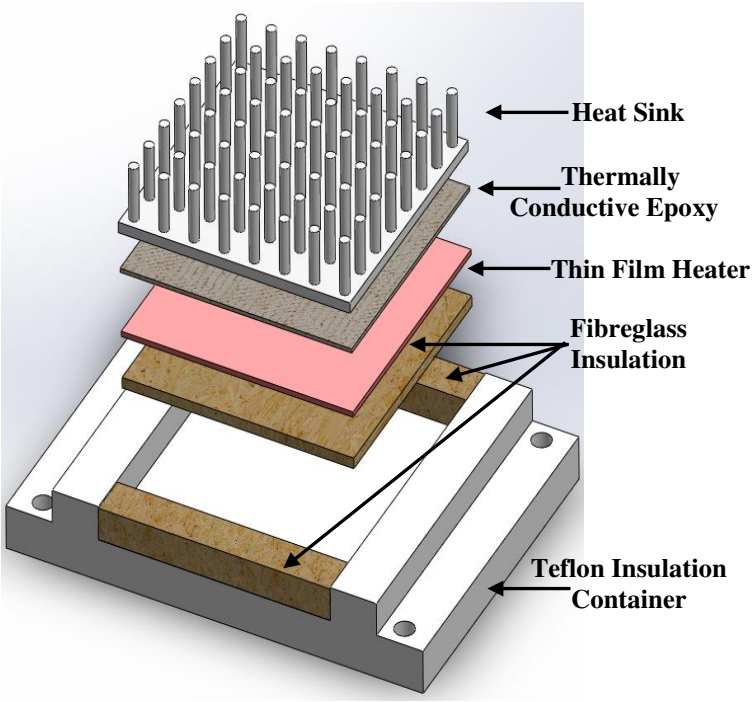

Figure 3: Installation of the heat sink with film heater into the insulation chamber.

3. NUMERICAL METHODS

3.1 Problem Specification

The PFHS configurations considered here are shown in Figures 4 and 5. Its base has dimensions 50mm x 50mm x 2mm and the pin sizes are based on the experimental heat sink design shown in Figure 2 with a 6.5mm pitch in both directions. In addition to the two experimental pin fins (referred to as 0 and 3P – see figure 4), the seven other pin designs in Figure 4 were considered (again with the perforations aligned in the direction of the flow). The porosities of the pin fins, defined as $\phi=V_{hole}/V$ where V_{hole}, and V are the volume of

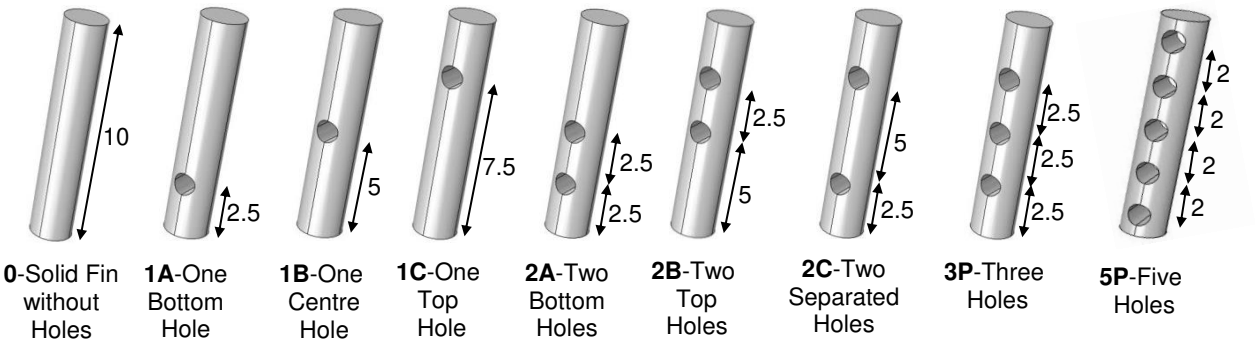

Figure 4: The nine pin fin designs considered, with various numbers and locations of perforations; all dimensions in mm.

3.2 Conjugate Heat Transfer Model

Thermal airflow through an aluminium PFHS is analysed using CFD. The inlet air temperature is set to 25°C and the inlet air velocity is varied between 6.5m/s and 12m/s leading to Reynolds numbers in the range 3500-6580 based on a length scale given by the hydraulic diameter of the duct D_h=2H.B/(H+B), where H and B are height and width of duct in which the heat sink is located, respectively. The airflow is assumed to be steady, incompressible and turbulent.

In the conjugate heat transfer model the rate of heat conduction through the aluminium heat sink is balanced by heat transfer by convection into the moving air stream, through a coupled boundary condition at the solid/fluid interface, as illustrated in Figure 5(a).

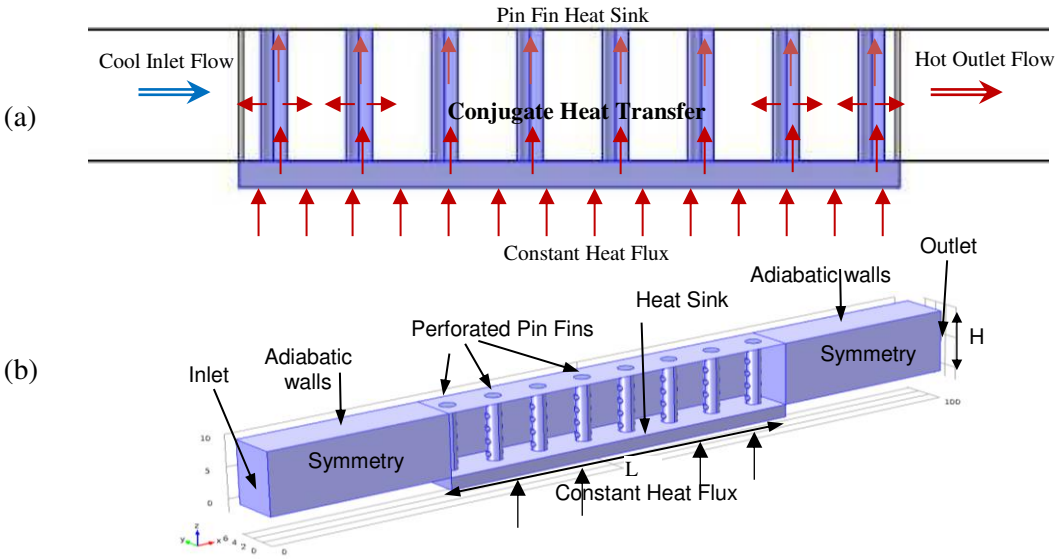

Figure 5: (a) Conjugate heat transfer model of the pin fin heat sink; (b) schematic diagram of the flow domain used in the CFD analyses, with eight perforated pin fins.

In the solid heat sink the temperature field T_s is obtained by solving the steady heat conduction equation

$$\nabla.(k_s \nabla T_s) = 0$$

where k_s=202W/mK is the thermal conductivity of the aluminium material used in the heat sink described previously.

Previous relevant studies have used the Reynolds-Averaged Navier-Stokes (RANS) equations to model turbulent flow through heat sinks successfully, see e.g. Zhou & Catton [3], Leung & Probert [26]. Time-averaging the continuity, momentum and energy equations with variables decomposed into mean and fluctuating components leads to the RANS equations, namely:

$$\nabla.\underline{U} = 0$$

$$\frac{\partial \underline{U}}{\partial t} + \nabla.(\underline{U}\,\underline{U}) = \frac{1}{\rho}\nabla.\left(\underline{\underline{\sigma}} - \rho\overline{\underline{U}'}\,\overline{\underline{U}'}\right)$$

where $\underline{\underline{\sigma}} = -p\underline{\underline{I}} + \mu\left(\nabla\underline{U} + \left[\nabla\underline{U}\right]^T\right)$ is the Newtonian stress tensor, μ is the air viscosity, ρ its density, $\underline{U}$ and $\overline{\underline{U}'}$ the average and turbulent fluctuation velocity vectors respectively, p is the pressure and $\underline{\underline{I}}$ the unit tensor. The incompressible RANS equations are solved with the energy equation for the temperature field in the fluid, T_f, with a heat source Q Watts, using the following equation

$$\frac{\partial T_f}{\partial t} + \underline{U}.\nabla T_f = \left(\frac{\nu}{\mathrm{Pr}} + \frac{\nu_t}{\mathrm{Pr}_t}\right)\nabla^2 T_f + \frac{Q}{\rho C_p}$$

where C_p is the specific heat capacity of the air, P_r and ν are the Prandtl number and kinematic viscosity of the air respectively and the subscript t indicates their turbulent counterparts.

Following Zhou & Catton [3] and Leung & Probert [26], the thermal airflow through the heat sink is modelled using the k-ω SST model with automatic wall function treatment. As discussed above and following Leung & Probert [26], who found that with temperature differences of 40°C and 77.5°C for polished aluminium fins, the radiative heat loss is less than 5% and 8%, respectively of total heat transfer rate, radiative heat transfer is neglected. Air density and viscosity are assumed to be constant and equal to those at the inlet temperature of 25°C. This model combines the accurate formulation of the k-ω model in the near-wall region with the free-stream independence of the k-ε one in the far field, and has been shown to predict highly separated flows accurately in a number of previous validation studies, Menter [27], Zhou & Catton [3].

The equations for the SST model are:

$$\frac{\partial(\rho k)}{\partial t} + \underline{U}.\nabla(\rho k) = \tilde{P}_k - \beta^*\rho k\omega + \nabla.\left[(\mu + \sigma_k\mu_t)\nabla k\right]$$

$$\frac{\partial(\rho\omega)}{\partial t} + \underline{U}.\nabla(\rho\omega) = \alpha\rho S^2 - \beta\rho\omega^2 + \nabla.\left[(\mu + \sigma_\omega\mu_t)\nabla\omega\right] + 2(1-F_1)\rho\sigma_{\omega_2}\frac{1}{\omega}\nabla k.\nabla\omega$$

where the blending function F_1 is defined by

$$F_1 = \tanh\left(\left\{\min\left[\max\left(\frac{\sqrt{k}}{\beta^* \omega y}, \frac{500\nu}{y^2 \omega}\right), \frac{4\rho\sigma_{\omega_2} k}{C D_{k\omega} y^2}\right]\right\}^4\right)$$

in which

$$C D_{k\omega} = \max\left(2\rho\sigma_{\omega_2} \frac{1}{\omega} \nabla k . \nabla \omega, 10^{-10}\right)$$

The turbulent eddy viscosity is computed from

$$\nu_t = \frac{a_1 k}{\max(a_1 \omega, S F_2)}$$

where S is the invariant measure of the strain rate and F_2 is a second blending function defined by

$$F_2 = \tanh\left(\left[\max\left\{2\frac{\sqrt{k}}{\beta^* \omega y}, \frac{500\nu}{y^2 \omega}\right\}\right]^2\right)$$

To limit the growth of turbulence in stagnation regions, a production limiter is used in the SST model.

$$P_k = \mu_t \frac{\partial u_i}{\partial x_j}\left(\frac{\partial u_i}{\partial x_j} + \frac{\partial u_j}{\partial x_i}\right) \rightarrow \tilde{P}_k = \min\left(P_k, 10\beta^* \rho k \omega\right)$$

The constants for this model are: $\beta^* = 0.09, \alpha_1 = \frac{5}{9}, \beta_1 = \frac{3}{40}, \sigma_{k1} = 0.85, \sigma_{\omega_1} = 0.5, \alpha_2 = 0.44,$

$\beta_2 = 0.0828, \sigma_{k2} = 1, \sigma_{\omega 2} = 0.856.$

A commercial Finite Volume Method-based code, ANSYS FLUENT [28] is used to solve the fully coupled momentum and energy equations, using second order upwinding, while continuity is satisfied using the SIMPLE method. The grid is composed of tetrahedral mesh elements to improve the quality of the numerical prediction near curved pin surfaces.

3.3 Boundary Conditions

The computational problem is reduced in size by exploiting the symmetry of the PFHS to apply symmetry boundary conditions (Table 1) along the sides of the channel so that the conjugate heat transfer model is solved for a system of eight pins aligned with the dominant flow direction, Figure 5(b). Along the bottom wall of the heat sink, a constant heat flux $\dot{Q}$=50W, used in the experiments, is applied and no-slip conditions Ux=Uy=Uz=0 are imposed along the heat sink walls. A pressure outflow boundary condition is imposed at the outlet boundary. All remaining walls are considered to be adiabatic.

Table 1: The boundary conditions of the conjugate heat transfer model

Locations	Fluid Conditions	Thermal Conditions	Locations	Fluid Conditions	Thermal Conditions
Inlet	6.5≤U≤12.2m/s	Tf=25°C	**Bottom wall of heat sink**	U=0	$\dot{Q}$=constant
Right and left sides (symmetry)	$\frac{du}{dy}=0$	$\frac{dT}{dy}=0$	**Pressure outlet**	p=0	$\frac{dT}{dx}=0$
Top wall and other walls	U=0	$\frac{dT}{dz}=0$	**Pin heat sink**	U=0	$kf.\frac{dTf}{dn}=ks.\frac{dTs}{dn}$

4. RESULTS AND DISCUSSION

4.1 Effect of Grid Density

Numerical solutions of the conjugate heat transfer model in the domain shown in Figure 5(b) are obtained on a series of grids for both a solid and a perforated pin fin cases. For the former, the number of cells is increased between 98,104 and 171,059, while for perforated pin fins (3P) the number of cells in increased between 113,000 and 202,678. The effect of grid resolution on Nu_T, T_{case} and Δp are shown in Table 2. For solid pin fins increasing the number of cells beyond 124,000 leads to a less than 3% variation in the quantities of interest, whereas for perforated pin fins, increasing the number of cells beyond 161,000 results in less than 3% variation in these parameters. All results reported below have used these appropriate levels of grid refinement for solid and perforated pin fin cases.

Table 2: Grid independence study data for solid and perforated pin fin heat sinks

Solid Pins (0) Cells	Nu_T	T_{case} (°C)	ΔP (pa)	Perforated Pins (3P) Cells	Nu_T	T_{case} (°C)	ΔP (pa)
98104	348.2	67.4	107.2	113000	373.6	63.0	92.7
134035	362.3	66.3	103.8	161916	395.2	61.3	93.6
171059	367.0	65.6	103.7	202678	400.0	61.7	95.2

4.2 Validation against Previous Studies

The Nusselt number and pressure drop predictions are now compared with those of Zhou & Catton [3] for flow past PFHSs with solid pin fins. Figure 6 compares predictions of Nu and pressure drop Δp across the pin fins. These both generally compare well with the prediction of Zhou & Catton [3] with typical discrepancies in the predictions of Nu and Δp of 3% and 5%, respectively. The predictions of the current CFD model are also compared against the experimental data of Sahin & Demir [1] for flow past a heat sink where the pin fins have a single perforation. Figure 7 compares CFD predictions of the ratio Nu/Nu_s (where $Nu_s=0.077\ Re^{0.716}\ Pr^{1/3}$ is Sahin & Demir's [1] experimental correlation for heat transfer from a smooth surface without pins) with their experimental data. Again, the agreement with the experimental data is generally good, with a maximum discrepancy of less than 7%.

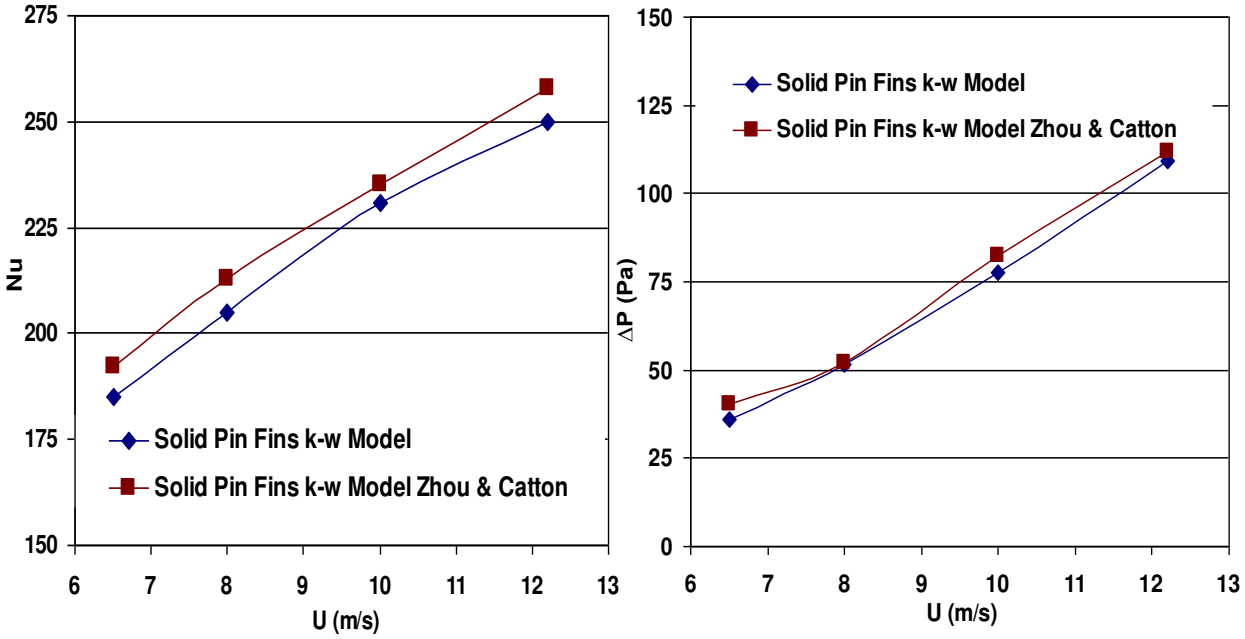

Figure 6: Comparison of Nusselt number, Nu, and pressure drop, Δp, predictions with those of Zhou & Catton [3].

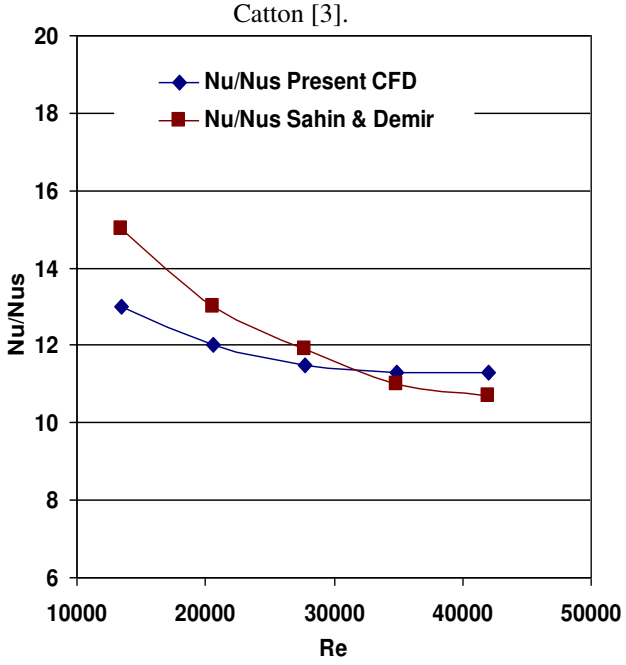

Figure 7: Comparison between CFD predictions of Nu/Nus with experimental data of Sahin & Demir (2008) for pin fins with a single perforation

4.3 Effect of Perforations on Pressure Drop and Fan Power Consumption in PFHSs

Figure 8 compares experimental measurements and numerical predictions from the present study into the effect of perforations on the pressure drop, Δp, across PFHSs and the fan power required to overcome the pressure drop, P_{fan}=UAΔp. Data is presented for both the solid pin 0P and 3P pin fins and the experimental bars represent the variation in the data over three repetitions of the experiments. The pressure drop data in Figure 8(a) shows that the perforations reduce Δp throughout the velocity range. In the experimental data, the pressure drop with three perforations is typically around 7% smaller than for solid pin fins, while for

the numerical predictions this reduction is approximately 9%. The experimental pressure drops are typically 10% higher than the numerical predictions and this may be due to the practical difficulties of fabricating PFHSs with several perforations. The latter may include discrepancies caused by minor misalignments of the perforations and finite perforation surface roughness, both of could increase the pressure drop significantly. The fan power data in Figure 8(b) shows the expected quadratic dependence on air speed, U, and again demonstrates the benefits of the 3P pin fins.

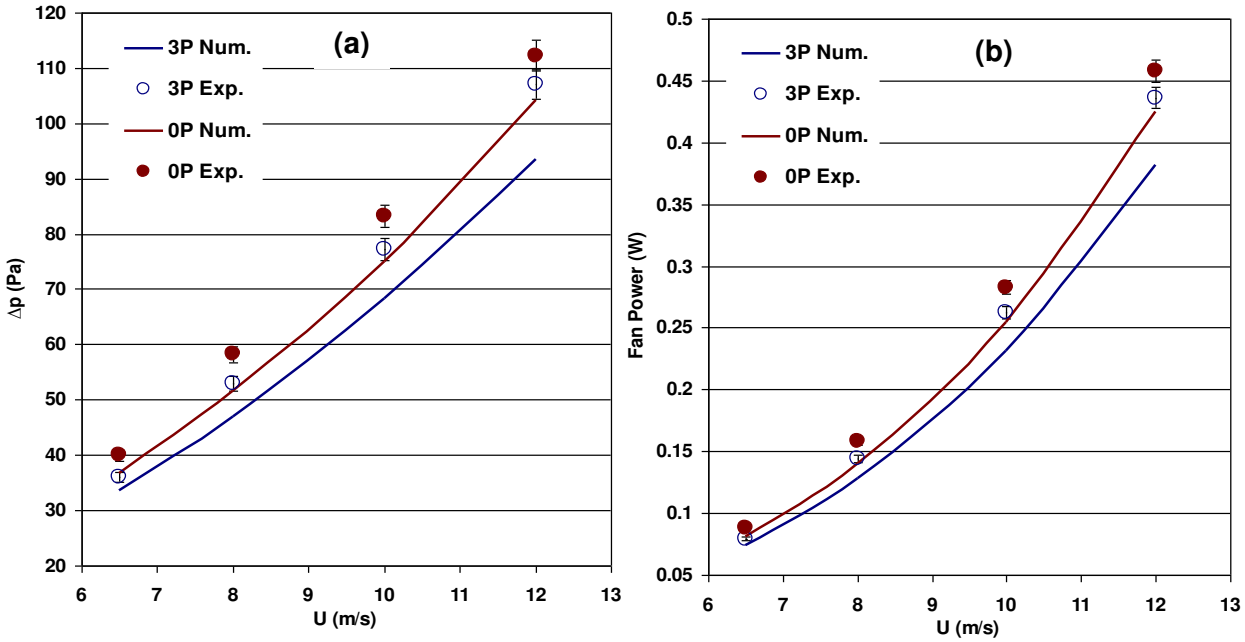

Figure 8: Effect of pin perforations on (a) pressure drop and (b) fan power as a function of airflow speed.

4.4 Effect on Heat Transfer

Since the overall design goal for PFHSs is to achieve a high heat transfer rate at the minimum energy cost, Figure 9 shows the corresponding experimental measurements and numerical predictions of Nusselt number, based on either the total PFHS wetted surface area, Nu_T, or on the projected surface area, Nu_P. The latter may perhaps be a more effective measure of cooling capacity for a given PFHS size. The data shows that both Nu_T and Nu_P increase approximately linearly with the inlet air velocity and that the 3P pin fin design achieves a significant enhancement in heat transfer, with Nu_T typically between 5% and 10% larger and Nu_P between 11% and 14% larger than for solid pin fins. Note that once again the experimental data is typically between 10% to 15% smaller than predicted numerically due to the practical considerations mentioned above. A further source of error for the heat transfer measurements may be due to the additional thermal resistance as a result of the brazing process, where the brazing material did not completely fill the gap between the pin and the base plate.

In many electronics systems, PFHSs provide the cooling needed to keep processor temperatures below critical temperatures where thermally-driven failure mechanisms,

including intermetallic growth, corrosion, metal migration and void formation, degrade reliability and reduce the mean-time-to-failure, Gurrum et al [29], Yuan et al [30]. Figure 10 compares experimental measurements and numerical predictions of the average PFHS base plate temperature, T_{case}, as a function of the fan power needed to overcome the pressure drop, for inlet air velocities in the range 6.5m/s≤U≤12m/s. Both sets of data show the consistent trend of requiring higher fan power in order to reduce T_{case} and that the improved heat transfer from the perforated pins (3P) leads to significantly lower CPU temperatures: the 3P perforated fins lead to CPU temperatures typically between 4 and 6°C lower than with solid pin fins, for the same fan power input.

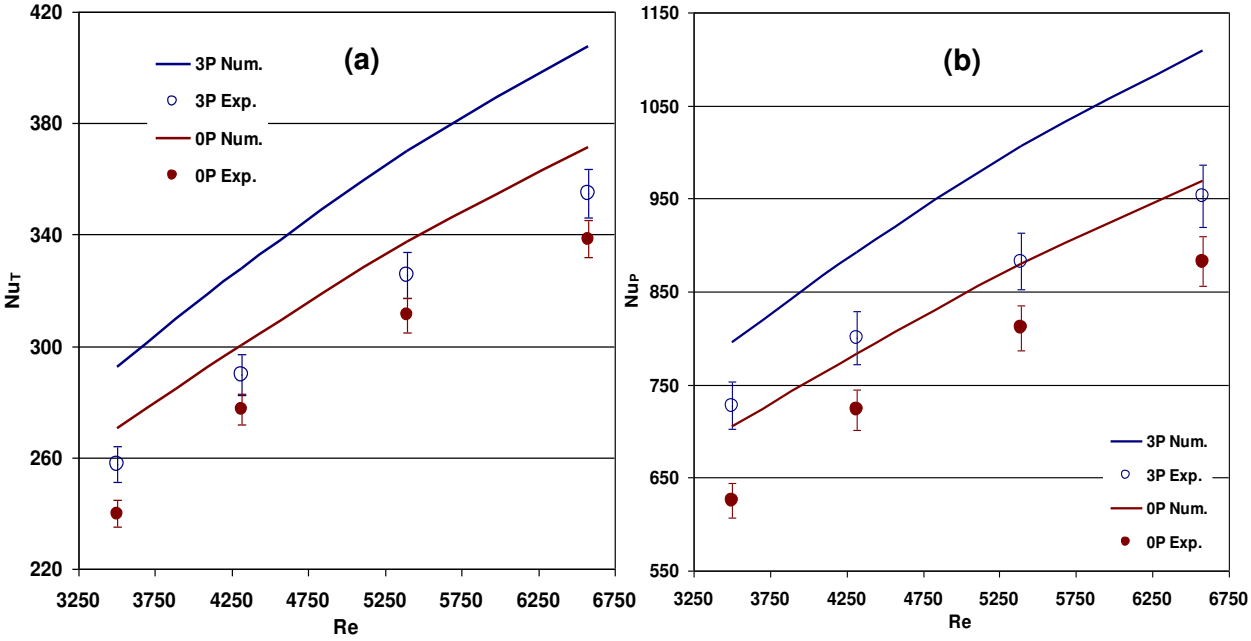

Figure 9: Effect of inlet velocity on Nusselt number based on A) total B) projected surface area

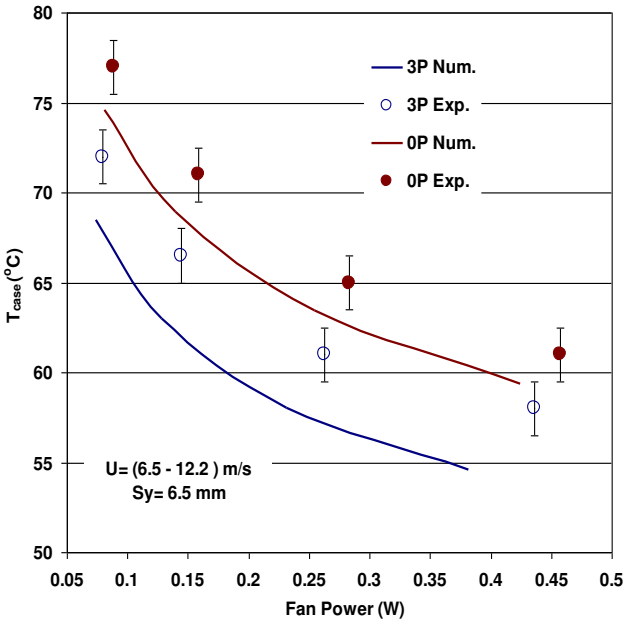

Figure 10: Comparison between experimental and numerical predictions of influence of fan power on T_{case}.

4.5 Numerical investigation of perforated PFHSs

The conjugate heat transfer model is now used to study thermal air flows past heat sinks with the nine pin designs shown in Figure 4, for inlet air velocities in the range 6.5m/s≤U≤12m/s, corresponding to 3500≤Re≤6580. Figures 11 and 12 show the results of more detailed studies into the effect of multiple pin fin perforations on Δp, fan power and Nu_T for PFHSs. Collectively they show that pressure drop decreases monotonically and Nu_T increases monotonically with the number of perforations. For a given inlet air velocity, the 5P pin fin design provides the highest heat transfer rate and the lowest pressure drop and fan power requirement. The pressure drop and Nu_T for the 5P pin fin are approximately 16% smaller and 11% higher, respectively, than for the solid pin case. These findings are consistent with the recent conclusions of Sara et al [31], which attributed improved heat transfer with perforations to the combined effects of increased surface area and the formation of localized air jets.

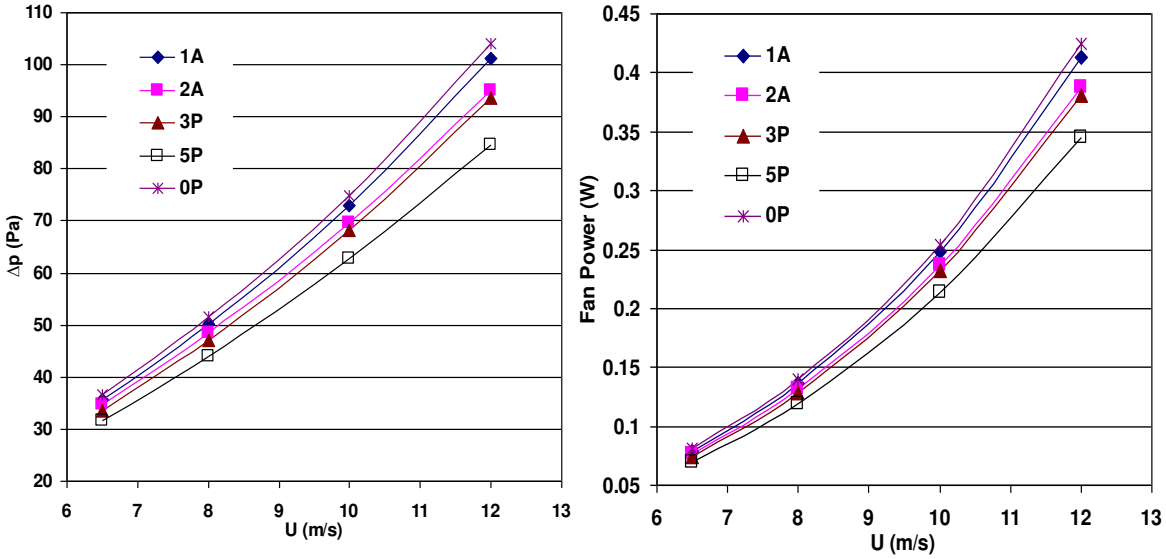

Figure 11: Effect of pin perforations and inlet velocity on pressure drop (left) and fan power (right).

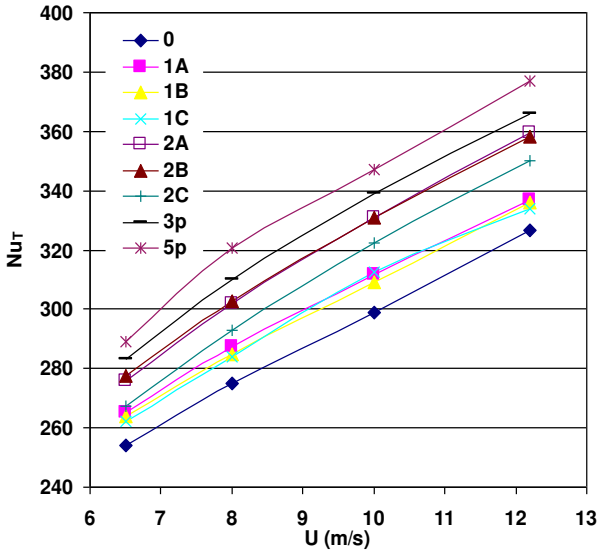

Figure 12: Effect of inlet velocity on Nu_T for the nine pin designs shown in Fig.1.

The position of the perforations is of secondary importance. The Nusselt number of the perforated pin fin designs 2A and 2B are slightly higher (typically up to 3% larger) than that of perforated pin (2C) design. This is probably due to stronger interactions between the airflow jets that are in closer proximity in cases 2A and 2B, see Figure 13, compared with those of the perforated pin, 2C.

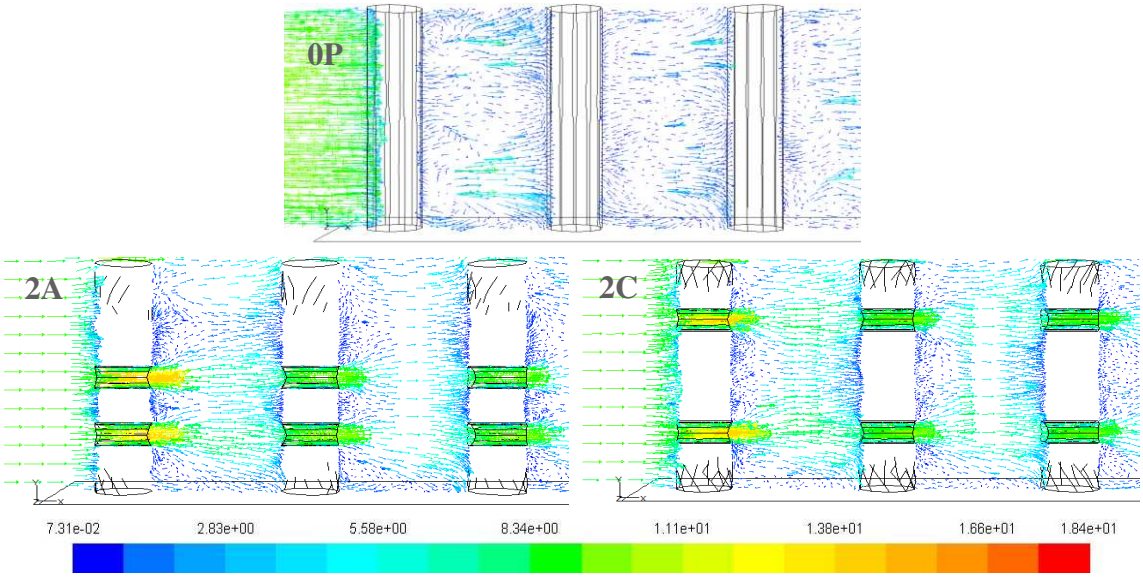

Figure 13: Comparison between predicted flow field in PFHSs with solid pin fins and for designs 2A and 2C with two perforations.

Figure 14 presents a more detailed investigation into the effect of pin fin perforations on the relationship between fan power and heat sink temperature. For a given fan power, the 5P perforation reduces the heat sink base plate temperature by a further 1-1.5°C compared to the 3P pin design. Figure 15 compares the surface temperatures of the solid pin fin heat sinks with those obtained with the 5P pin fins. In the former case, temperatures on the base plate vary between approximately 58.5°C and 71°C, whereas for the perforated pins the corresponding temperatures vary between approximately 49.5°C and 65°C. The temperatures on the pins are also significantly cooler, as indicated by the greater preponderance of blue regions on the perforated pins.

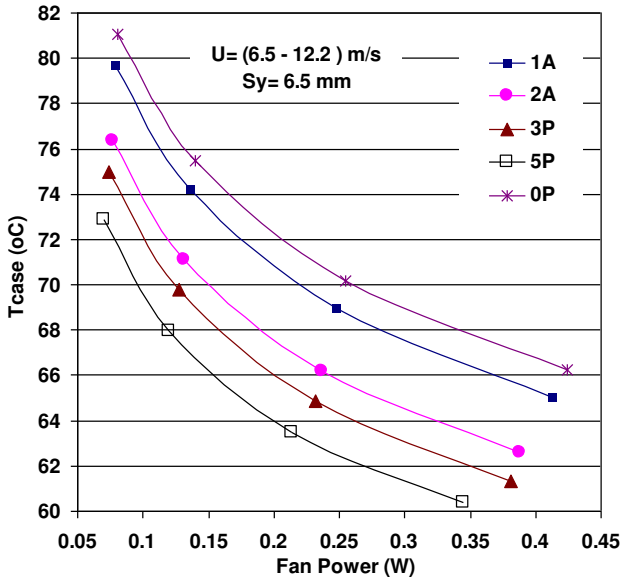

Figure 14: Effect of pin design and pumping power on $T_{case,ave}$

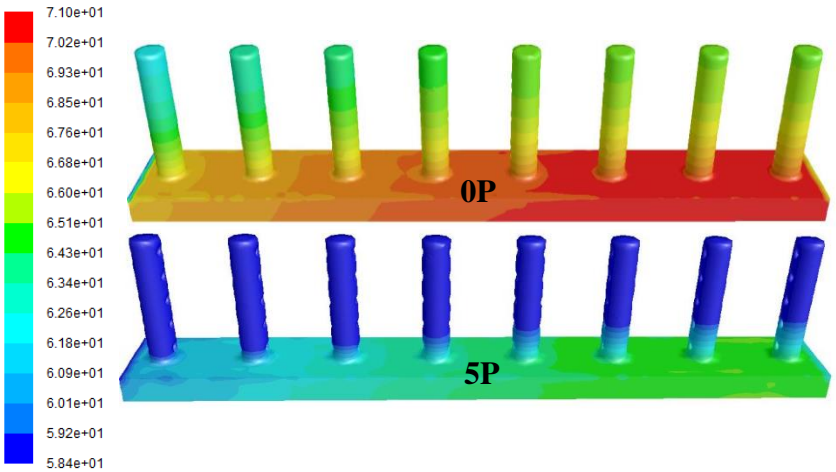

Figure 15: Temperature distribution through pinned heat sinks: 0P and 5P models at Re=5393

The final sets of results consider the effect of the density of distribution of pins over the heat sink surface. Figures 16 and 17 show the effect of the number of rows of pins on Nu_T and Δp respectively, for a range of Reynolds numbers; once again, each row has 8 equally spaced pins, with uniform spacing between each row in the flow direction. Figure 16(a) shows that for solid pins Nu_T increases monotonically with the number of rows and the variation is quite small (of the order of 5%). Note, however, that the total area A_T is increasing significantly and the values of Nu_P typically double as the number of rows is varied between 4 and 11. For perforated (3P) pins there are well-defined maxima corresponding to 6 rows of pins. This is probably due to the important interactions between the jets flows through the pins being restricted when pins at packed too tightly.

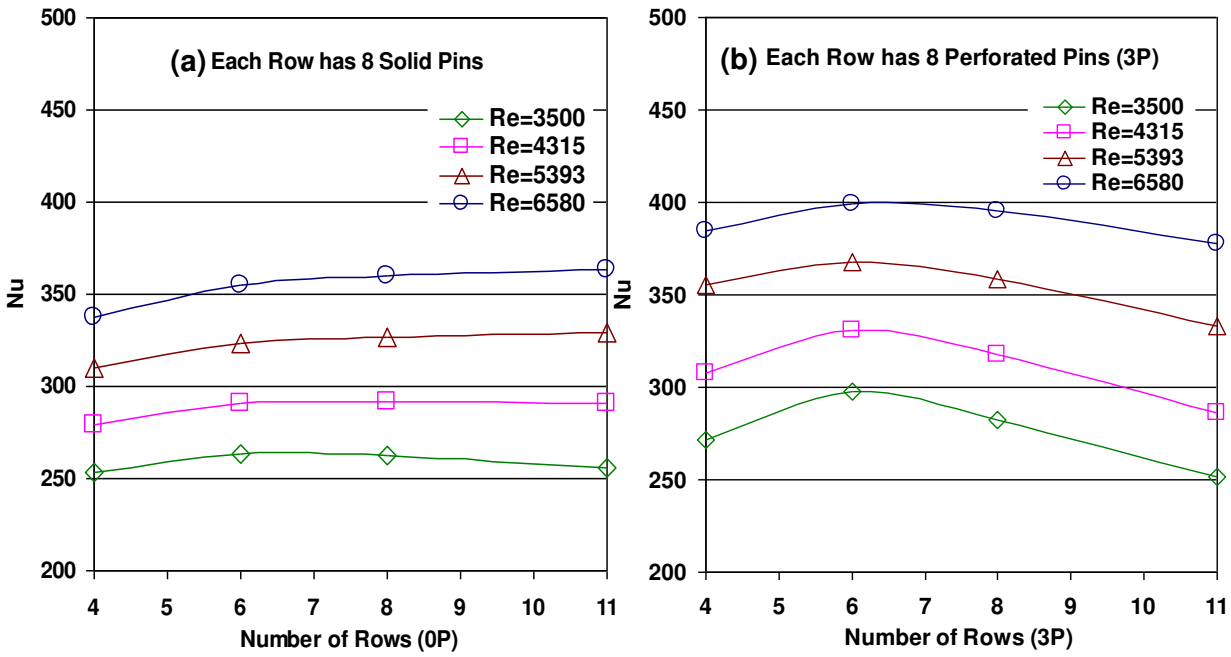

Figure 16: Effect the number of rows on the Nusselt number Nu_T with variation Reynolds number for both (a) solid (0P) and (b) perforated (3P, right) pinned heat sinks models

Figure 17 shows the corresponding data for pressure drop across the heat sink. As expected, increasing the pin packing density increases Δp for both the solid and perforated pins. In both cases, halving the number of rows from 8 to 4 would reduce Δp by approximately 35%.

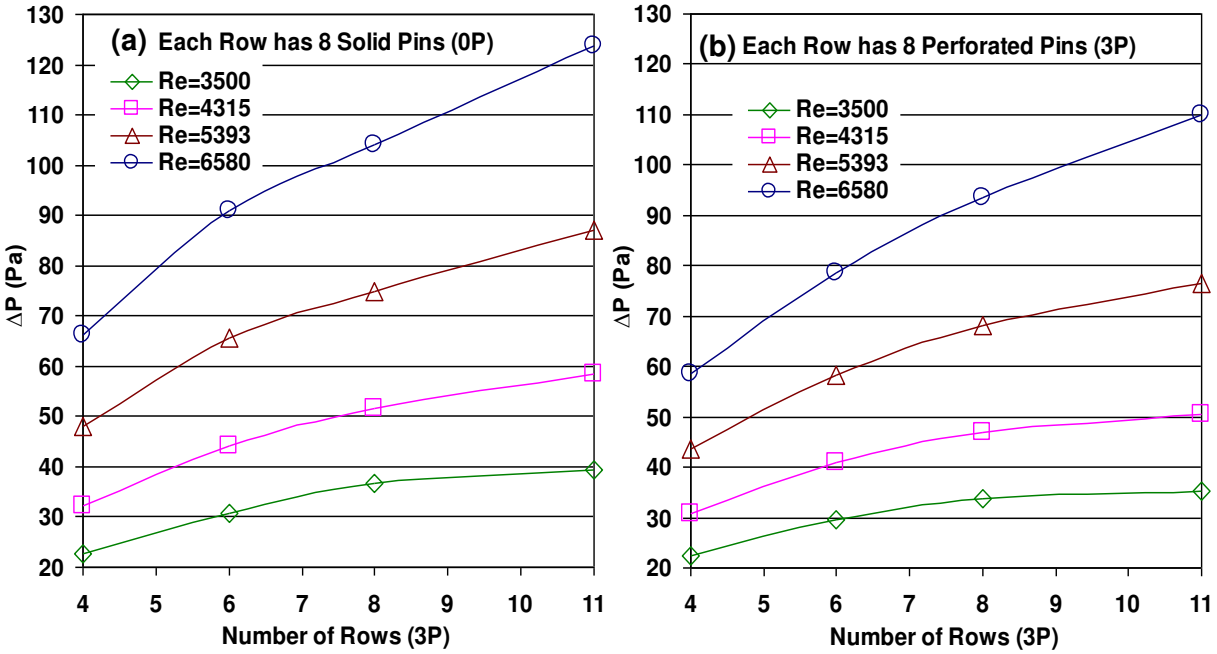

Figure 17: Variation of pressure drop with the number of rows on and different Reynolds number for (a) solid (0P) and (b) perforated (3P) pinned heat sinks models.

Finally, the effect of pin density on the CPU temperature and fan pumping power are shown in Figure 18. Results are plotted with respect to a reference critical temperature of 85°C, a typical maximum temperature CPU temperature for reliable operation of a desktop PC, Yuan et al [30].

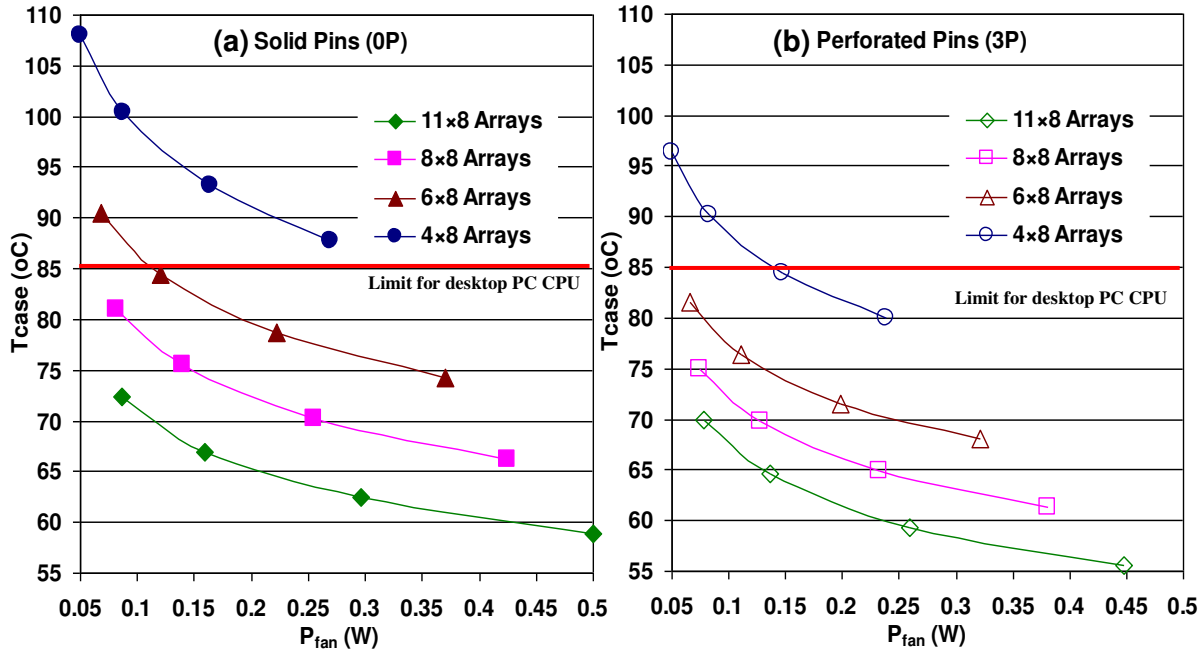

Figure 18: Effect the number of rows on the CPU temperature and fan power (a) solid (0P) and (b) perforated (3P) pinned heat sinks models.

The results show that the increased conduction heat transfer from the CPU, resulting from the higher pin densities, means that the CPU can be cooled below the critical temperature for a significantly lower fan power input, P_{fan}. For the solid pins, a fan power of 0.1W enables the CPU temperature to be maintained below 73^{o}C when 11 rows of pins are used whereas for 4 rows the CPU temperature of 100^{o}C is well above the critical CPU temperature. Using rows of 3P perforated pins reduces the CPU temperature yet further, for a given fan power input, and even makes the adoption of 4 rows of perforated pins viable for fan power inputs above 0.15W. These results also demonstrate that care must be taken when extrapolating from the Nusselt number data given in Figure 16.

5. CONCLUSIONS

Pin fin heat sinks provide cooling for critical components in many important applications, ranging from aero engines and nuclear reactors to computers and other microelectronic devices, where inexorable increases in power densities are driving innovation in heat exchange techniques. Whilst some of this innovation in IT systems is focussing around on the use of liquid cooling (e.g. on-chip cooling technologies, such as the Aquasar system, or dielectric liquid immersion cooling, [32, 33], the use of convective heat transfer to air as it passes over extended surface heat sinks will remain popular since it provides high reliability cooling at relatively low cost, Zhou & Catton [3].

The present study has shown that the use of multiple pin perforations can have substantial performance benefits by enabling the heat transfer to be increased while at the same time reducing both the pressure drop across the heat sink and fan power needed to pump the air through them. The Nusselt number increases monotonically with the number of pin perforations while the pressure drop and fan power both reduce monotonically. For the cases considered here, pins with five perforations have a Nusselt number and pressure drop typically 11% and 16% respectively, larger compared to heat sinks with solid pins. The experimental work has also been extremely valuable in highlighting the practical difficulties of using densely distributed pin fins with multiple perforations. It showed that to maximise the benefits from perforations care must be taken to ensure that they are aligned with the dominant flow direction and manufactured with a good quality surface finish. These factors add cost and complexity to manufacturing processes and research is currently ongoing into addressing these practical issues.

ACKNOWLEDGEMENTS

The authors would like to thank the Higher Committee for Education Development in Iraq (HCED), Iraqi Ministry of Higher Education and Scientific Research (MOHE), and Mechanical Engineering Department University of Anbar, Iraq for financial support of this work.

REFERENCES

1. Sahin, B. and A. Demir, Thermal performance analysis and optimum design parameters of heat exchanger having perforated pin fins. Energy Conversion and Management, 2008. 49(6): p. 1684-1695.
2. Sahin, B. and A. Demir, Performance analysis of a heat exchanger having perforated square fins. Applied Thermal Engineering, 2008. 28(5-6): p. 621-632.
3. Zhou, F. and I. Catton, Numerical Evaluation of Flow and Heat Transfer in Plate-Pin Fin Heat Sinks with Various Pin Cross-Sections. Numerical Heat Transfer, Part A: Applications, 2011. 60(2): p. 107-128.
4. N. Nagarani, K.Mayilsamy, A.Murugesan, G.Sathesh Kumar. Review of utilization of extended surfaces in heat transfer problems. Renewable and Sustainable Energy Reviews, 2014. 29, 604-613.
5. K.T Chiang. Optimization of the design parameters of parallel-plain fin heat sink module cooling phenomenon based on the Taguchi method. Int. Comm. Heat and Mass Transfer, 2005. 32(9), 1193-1201.
6. Soodphakdee D, Behnia M, and Copeland D. W. A Comparison of Fin Geometries for Heat Sinks in Laminar Forced Convection Part I: Round Elliptical, and Plate Fins in Staggered and In-Line Configurations The International Journal of Microcircuits and Electronic Packaging, 2001. 24, 68-76.
7. Jonsson, H., & Moshfegh, B., Modeling of the thermal and hydraulic performance of plate fin, strip fin, and pin fin heat sinks-influence of flow bypass. Components and Packaging Technologies, IEEE Transactions on, 2001. 24, 142-149.
8. Yang, Y.T. & Peng, H.S., Investigation of planted pin fins for heat transfer enhancement in plate fin heat sink. Microelectronics Reliability, 2009a. 49, 163-169.
9. Yang, Y.T. & Peng, H.S., Numerical Study of Thermal and Hydraulic Performance of Compound Heat Sink. Numerical Heat Transfer, Part A: Applications, 2009b. 55, 432-447.
10. M.R. Hajmohammadi, V. Alizadeh Abianeh, M. Moezzinajafabadi, M. Daneshi, Fork-shaped highly conductive pathways for maximum cooling in a heat generating piece. Applied Thermal Engineering, 2013, 61, pp 228-235.
11. M. R. Hajmohammadi, M. Moulod, O. Joneydi Shariatzadeh &A. Campo, Effects of a Thick Plate on the Excess Temperature of Iso-Heat Flux Heat Sources Cooled by Laminar Forced Convection Flow: Conjugate Analysis. Numerical Heat Transfer, Part A, 2014, 66, pp 205-216.
12. H. Najafi, B. Najafi, P. Hoseinpoori, Energy and cost optimization of a plate and fin heat exchanger using genetic algorithm. Applied Thermal Engineering, 2011, 31, pp 1839-1847.
13. I. Kotcioglu, A. Cansiz, M. Nasiri Khalaji, Experimental investigation for optimization of design parameters in a rectangular duct with plate-fins heat exchanger by Taguchi method. Applied Thermal Engineering, 2013, 50, pp 604-613.
14. P. Kumar Das & I. Ghosh, Thermal Design of Multistream Plate Fin Heat Exchangers—A State-of-the-Art Review. Heat Transfer Engineering, 2012, 33(4-5), 284-300.
15. Shaeri, M.R. and M. Yaghoubi, Thermal enhancement from heat sinks by using perforated fins. Energy Conversion and Management, 2009. 50(5): p. 1264-1270.
16. Shaeri, M.R. and M. Yaghoubi, Numerical analysis of turbulent convection heat transfer from an array of perforated fins. International Journal of Heat and Fluid Flow, 2009. 30(2): p. 218-228.
17. Shaeri, M.R. and T.C. Jen, The effects of perforation sizes on laminar heat transfer characteristics of an array of perforated fins. Energy Conversion and Management, 2012. 64: p. 328-334.
18. Shaeri, M.R. and T.C. Jen, Turbulent Heat Transfer Analysis of a Three-Dimensional Array of Perforated Fins Due to Changes in Perforation Sizes. Numerical Heat Transfer, Part A: Applications, 2012. 61(11): p. 16.
19. Ismail, F., Effects of Perforations on the Thermal and Fluid Dynamic Performance of a Heat Exchanger. IEEE Transaction on Component, Packaging and Manufacturing Technology, 2013. p.1-8.

20. Md. Farhad Ismail, M.O. Reza, M.A. Zobaer, and Mohammad Ali, Numerical investigation of turbulent heat convection from solid and longitudinally perforated rectangular fins. IEEE 5th BSME International Conference on Thermal Engineering, 2013. p.497-502.
21. K. H. Dhanawade and H. S. Dhanawade, Enhancement of Forced Convection Heat Transfer from Fin Arrays with Circular Perforation. IEEE, Frontiers in Automobile and Mechanical Engineering (FAME), 2010. p. 192-196.
22. Amol B. Dhumme and Hemant S. Farkade, Heat Transfer Analysis of Cylindrical Perforated Fins in Staggered Arrangement. International Journal of Innovative Technology and Exploring Engineering (IJITEE), 2013. 2(5): p. 225-230.
23. Dai, X., F. Yang, R. Fang, T. Yemame, J.A. Khan, and C. Li.. Enhanced single- and two-phase transport phenomena using flow separation in a microgap with copper woven mesh coatings. Applied Thermal Engineering, 2013. 54 (1): 281-288.
24. Naik, S., S.D. Probert, and M.J. Shilston. Forced-convective steady-state heat transfers from shrouded vertical fin arrays, aligned parallel to an undisturbed air-stream. *Applied Energy,* 1987. 26 (2): 137-158.
25. Şara, O.N. 2003. Performance analysis of rectangular ducts with staggered square pin fins. *Energy Conversion and Management.* 44 (11): 1787-1803.
26. Leung, C. W., & Probert, S. D., Heat-exchanger performance: effect of orientation. Applied energy, 1989. 33(4), 235-252.
27. Menter, F. R., Zonal Two Equation k-ω Turbulence Models for Aerodynamic Flows, AIAA 1993, p.93-2906.
28. ANSYS FLUENT User's Guide, 2011.
29. S. P. Gurrum, S. K. Suman and J. Y. K., Thermal Issues in Next-Generation Integrated Circuits, IEEE Transactions on device and materials reliability, 2004, vol. 4, no. 4, pp. 709-714
30. Yuan, W., Zhao, J., Tso, C. P., Wu, T., Liu, W. & Ming, T., Numerical simulation of the thermal hydraulic performance of a plate pin fin heat sink. Applied Thermal Engineering, 2012. 48, 81-88.
31. O. N. Sara, T. Pekdemir, S. Yapici and H. Ersahan, Thermal Performance Analysis for Solid and Perforated Blocks Attached on a Flat Surface in Duct Flow. Energy Conversion & Management, 2012. 41(10): p. 1010-1028.
32. Hopton, P. and Summers, J., Enclosed liquid natural convection as a means of transferring heat from microelectronics to cold plates. 29th IEEE Semiconductor Thermal Measurement and Management Symposium, 60-64, DOI: 10.1109/SEMI-THERM.2013.6526806.
33. IBM, Zurich, http://www.zurich.ibm.com/st/energy/zeroemission.htm.
34. Holman, J. P.. Experimental Methods for Engineers, McGraw Hill Book Company, 10971, 8th edition, 2011.